



ELSEVIER

Contents lists available at ScienceDirect

## Ocean Engineering

journal homepage: [www.elsevier.com/locate/oceaneng](http://www.elsevier.com/locate/oceaneng)

# Experimental and numerical characterization of harbor oscillations in the port of Málaga, Spain



S. Sammartino\*, J.C. Sánchez Garrido, J. Delgado, C. Naranjo,  
F. Criado Aldeanueva, J. García Lafuente

Physical Oceanography Group, University of Málaga, Campus de Teatinos s/n, 29071 Málaga, Spain

## ARTICLE INFO

## Article history:

Received 29 January 2014

Accepted 22 June 2014

Available online 11 July 2014

## Keywords:

Harbor resonance

Sea level oscillations

Resonance modes

MITgcm

## ABSTRACT

The port of Málaga is routinely affected by short period sea level oscillations whose amplitudes, typically of few cm, can sporadically outweigh the tidal variations. High frequency oscillations in the innermost basins may cause problems of stability of the moored crafts. This motivated the characterization of the resonant behavior of the port and its response to external forcing, which has been carried out by experimental and numerical approaches. The Helmholtz mode of the harbor has been found at ~16.5-min period, in both observed data and numerical experiments. A second mode of period around 6–7 min, beyond the temporal resolution of the tide gauge, has been detected only in the numerical results. The typical scenario during the occurrence of harbor oscillations is a low atmospheric pressure (75% of the cases) with noticeable content of high frequency pressure disturbances, a situation that is quite commonly observed during the transit of atmospheric fronts across the Iberian Peninsula. Winds appear to be of secondary influence, even when the oscillations are preferably observed under westerlies. Although results are not conclusive, resonance mechanisms (Proudman and Greenspan resonance) for transferring energy from the atmosphere to the ocean are proposed as the physical process generating the harbor oscillations.

© 2014 Elsevier Ltd. All rights reserved.

## 1. Introduction

The Port of Málaga is located in the middle of the Málaga Bay, facing to the Alboran Sea, at the southwestern margin of the Mediterranean Sea (Fig. 1). It has a relevant role in the commercial economy of the Spanish region of Andalusia, competing with the bigger infrastructures of the ports of Algeciras (Strait of Gibraltar) and Tanger-Med (Tangier, Morocco), but it is mostly devoted to touristic activities as shipping cruise and watercraft facilities. The Port has registered around 1 million passengers in 2011 (<http://www.malaga-port.net/publicaciones.html>) from international cruises, regular shipping lines and private nautical tourism.

Since 1997 the port has undergone a series of massive structural reforms such as the building of the eastern breakwater in 1997 and the container terminal in 1999 (Fig. 1b), which has noticeably increased its overall length and improved its commercial capabilities. Currently the local Port Authority is working out a plan to enhance the receptivity of small and medium ships, yachts and boats by installing new docks and facilities in the inner basins of the port. However they have to face problems of stability of the

moored crafts due to high frequency and small amplitude sea level oscillations that might well raise undesirable nuisance to potential users and, therefore, put the foreseen plan in question.

To a lesser extent, the observed situation in the port of Málaga recalls the well-known phenomenon of the ‘rissaga’ in Menorca Island in the Spanish Balearic Archipelago (Monserrat et al., 1991, 2006; Monserrat and Thorpe, 1992; Gomis et al., 1993; Garcies et al., 1996), the ‘marrobbio’ in Sicily (Candela et al., 1999) or the ‘abiki’ in Japan (Hibiya and Kajiura, 1982), where particular conditions of multiple resonances and a hazardous coupling between atmosphere and ocean induce catastrophic sea level oscillations (surges) causing associated damages for millions of dollars. Rabinovich (2009) describes this kind of phenomena as ‘harbor oscillations’, differentiating it from the well-known ‘seiches’. The latter are water level oscillations of closed basins, typically lakes, induced by the direct action of external meteorological or seismic forcing. The input disturbances trigger a series of oscillations of the surface with different frequencies, which depend on the geometry of the basin, and amplitude, which depends on the energy transferred from the external force. The energy transfer in turn is a function of the strength of the external force and, more importantly, the prevailing frequency, which may eventually lead to resonance. Friction and gravity gradually restore the equilibrium afterwards.

\* Corresponding author. Tel.: +34 952 13 28 49.

E-mail address: [ssammartino@ctima.uma.es](mailto:ssammartino@ctima.uma.es) (S. Sammartino).



**Fig. 1.** Panel (a) map of the Province of Málaga. Weather stations are represented in white circles. The main rivers and geographical structures cited in the work are indicated. Panel (b) map of the Port of Málaga. The two tide gauges analyzed are represented in white triangle.

The harbor oscillations, or coastal seiches (Drago, 2008), concern semi-enclosed basins (harbors, inlets or bays) and are generated by the arrival of long waves coming from the open sea. Many of them are the so called infragravity waves (Chen et al., 2004). Multiple resonance may occur during the energy transfer from the atmosphere to the sea surface and from the open sea to the harbor, while the main mechanism of dissipating this energy is by radiation through the open boundary (Rabinovich, 2009). A relevant issue in harbor oscillations is the associated currents (harbor currents) that can generate further resonance and possibly damages to the moored ships (Sawaragi and Kubo, 1982).

The present work aims at investigating the dynamic response of the port of Málaga to the external forcing and the possible generation of coastal seiches and high frequency sea level oscillations. The paper is organized as follows: Section 2 presents the experimental datasets. The harbor oscillations are characterized in Section 3 from the observations, while the theoretical and numerical treatment of the harbor dynamics is the subject of Sections 4 and 5. Section 6 investigates the atmospheric forcing for the occurrence of the events and, finally, Section 7 presents the conclusions. Appendix A provides details on the numerical experiments discussed in the work.

## 2. Available datasets

### 2.1. Sea level

Sea level data were provided by the Spanish State Port Authority (Puertos del Estado, PdE hereinafter), which has had two different tide gauges installed inside the port of Málaga. The oldest one, based on ultrasonic technology, was placed on the inner dock of a small marina along the eastern edge of the harbor and was working from July 1992 to April 2010, storing data every 5 min (PdE 5 min in Fig. 1b). In January 2009, a new tide gauge based on radar technology was installed on the corner of dock 6–7 at the opposite side of the harbor (PdE 1 min in Fig. 1b), measuring the sea level every minute. Both of them are part of the REDMAR sea level network of PdE ([http://calipso.puertos.es/BD/informes/INT\\_REDMAR.pdf](http://calipso.puertos.es/BD/informes/INT_REDMAR.pdf)).

The two series together span over more than 20 years and they have very few gaps (4.5% and 2.3% for the 1 and 5 min series, respectively). The series overlap from the end of January 2009 to the end of April 2010.

### 2.2. Meteorological variables

Four daily observations of atmospheric pressure and wind direction and speed at 0:00, 07:00, 13:00 and 18:00 h have been retrieved from the Spanish Meteorological Agency (AEMET) stations of Málaga Airport and Málaga Port. The time series of the Airport station span from January 1992 to October 2013 while the Port station has different lengths for atmospheric pressure (January 2006 to December 2009) and wind (January 2001 to October 2013). Another time series with a higher sampling rate of 15 min has been collected at a third station located at the Málaga University premises and covers the period November 2010 to November 2013 (GOFIMA series). Pressure and wind speed are given in hPa and  $\text{km h}^{-1}$ , with a resolution of 0.1 hPa and  $1 \text{ km h}^{-1}$ , respectively. Wind speed and direction have been converted in zonal and meridional velocity components.

To have an unbiased vision of the large-scale wind field free of topographic influences, daily gridded sea surface wind ASCAT (Advanced SCATterometer) observations with spatial resolution of  $0.25^\circ$  have been downloaded from <http://cersat.ifremer.fr/> (Bentamy and Croize-Fillon, 2012). Three cells around the city of Málaga have been averaged to obtain a single wind velocity series of years 2008 and 2009 with daily values.

Fig. 2 shows the wind roses of the different datasets. The regional wind regimen is clearly bidirectional, with slight prevalence of westerlies (Fig. 2a). Large-scale winds are conveyed by the local topography, which features marked river valleys oriented NW–SE, specially the Guadalhorce river (Fig. 1). The first and third quadrants are shielded by “El Torcal” formation and the Ronda chain (Muñoz, 1998), enclosing the so called “Málaga hole” (a flat depression around the urban nucleus and the valley of the Guadalhorce river) by the northeast and east-southeast, respectively (Fig. 1a). It results in the well-known bi-directionality of winds observed in Málaga area (Fig. 2b and c), with an overall slight predominance of WNW–NW winds, typical of autumn–winter, over SSE–SE winds, typical of spring–summer.

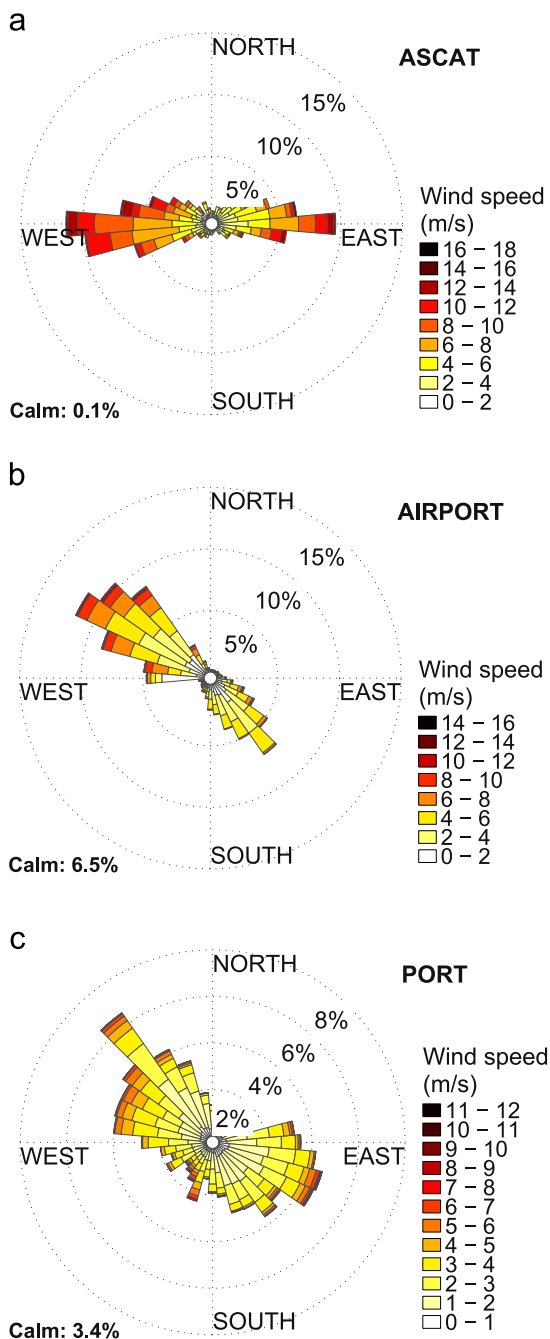


Fig. 2. Wind roses of ASCAT data (panel (a)), and the Airport (b) and Port (c) weather stations.

### 3. Short period harbor oscillations

The high frequency oscillations observed inside the Málaga harbor are of few cm amplitude and some tens of minute period. They must be compared with the tidal oscillations, which have amplitudes of 19.2 and 7.3 cm for M2 and S2 constituents, respectively, according to the output of the harmonic analysis performed on the whole time series. Therefore semidiurnal amplitudes are typically 12 cm in neap tides, and 26 cm during spring tides. As a rule, the high frequency oscillations are much weaker although they can reach and exceed tidal fluctuations under certain circumstances if they are suitably excited by external forces.

Fig. 3 shows the power spectra of the two sea level series available during their common period (20 of January 2009 to 23 of

April 2010). The 1 min series (PdE1 hereinafter) shows slightly higher amplitude than the 5 min series (PdE5), especially at the high-frequency end of the spectrum, the difference likely stemming from the different location of the instruments. The PdE1 tide gauge is in the main channel of the harbor, while the PdE5 gauge is sheltered in a small and shallower semi-enclosed basin with a narrow entrance (Fig. 1).

The analysis of short period oscillations has been carried out on the longer PdE5 series. A number of 17 complete years (from 1 of January 1993 to 31 of December 2009) has been selected in order to avoid seasonal biases in the statistical analysis. The data gaps have been filled in following two different approaches: (1) a linear interpolation whenever the gap was shorter than 6 samples (half an hour) and (2) a reconstruction of the tidal oscillations using the harmonic constants calculated by harmonic analysis (Pawlowicz et al., 2002) applied to the whole series, in case of gaps larger than 6 samples.

Harbor oscillations are location dependent and its main features are related to the interaction of local dynamics with the harbor structure. However, they are characterized by an enhancement of energy at the highest frequencies (Rabinovich, 2009). The spectrum in Fig. 3 reveals three more energetic bands around 16.5, 20.9 and 35.6 min. In order to discriminate their energy content, a series of FIR equi-ripple band-pass filters (Parks–McClellan algorithm, Oppenheim and Schaffer, 1999) have been applied to the series. This kind of filter assures a very weak distortion of the signal around the pass and stop frequencies.

The analysis mainly focuses on the band centered at 16.5 min period. The harbor oscillations are characterized on the basis of a standard deviation-threshold method. A 1-h width moving window has been applied to estimate the variance within every one-hour fragment along the whole PdE5 series and the short period oscillation events have been defined as those having a variance exceeding twice the standard deviation of the whole series ( $2\sigma$ ). The number of fragments exceeding such threshold represents around the 3% of the overall series and the number of ‘day with at least one event’ (DOE hereinafter) sum up the 18.6% of the whole period. They exhibit little seasonality and high interannual variability, as shown in Fig. 4b.

The average amplitude is nearly constant throughout the year (around 2 cm, color filled bars in Fig. 4a), although slightly higher amplitudes are found in the summer months (the highest mean amplitudes are in July). The maximum observed amplitude (white filled bars in Fig. 4a) may be as high as six times the average amplitude and it also has a tendency to show higher amplitudes in summer and lower amplitudes in winter. Superimposed to this seasonal variability, the interannual variability is much more evident: during the first five years of the series (the first five darkest color tones), the amplitudes are highly variable, alternating months of relatively great oscillations (January 1993 or July 1993/1994), with others with no events at all (March or April 1993–1998). In the year 1999 things seems to change radically, with a quite stable regimen throughout the rest of the series. Maxima indicates some kind of dome-shaped pattern, especially in the spring-summer months, with the highest peaks concentrated in the years 2002–2004, while the winter months show concentration of higher peaks in the last years of the series.

This situation is usually, but not always, confirmed by the distribution of the DOE (Fig. 4b). The events are more abundant in the spring-summer months (May and July) and at the end of the year (notice that the number of events is nearly one per day in December 2002), confirming the peak amplitude pattern. On the other hand, the highest maxima of July do not coincide with a higher density of events, which are more abundant in the last months of the series, especially in years 2002/2003. For instance, July 2004 presents one of the greatest averaged oscillations of the

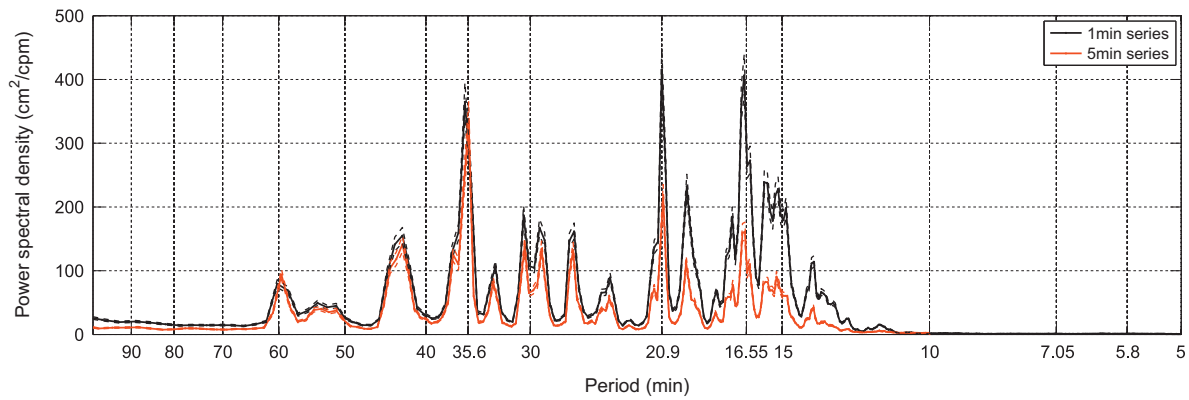


**Fig. 3.** Power spectra of the PdE1 series (black line) and the PdE5 series (red line). Dashed lines indicate 95% confidence limits. (For interpretation of the references to color in this figure legend, the reader is referred to the web version of this article.)

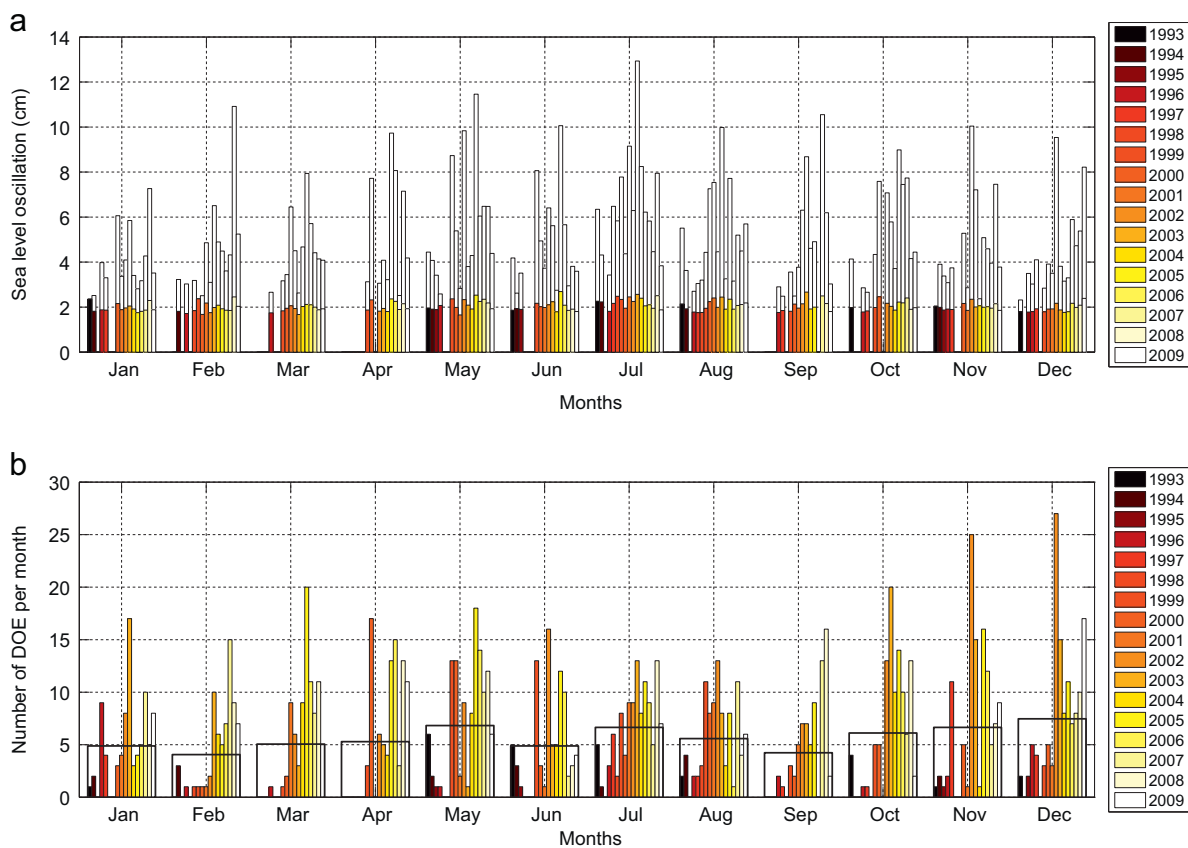


**Fig. 4.** Panel (a) monthly average (color filled bars) and maxima (white bars) amplitude of short period oscillations. Panel (b) number of events per month (color filled bars) and its interannual averages (thick empty bar). (For interpretation of the references to color in this figure legend, the reader is referred to the web version of this article.)

series and the highest of all peaks, while the number of events is relatively small with respect to the rest of the years (especially after 1999). On the other hand, while October 2003 is among the months with the highest abundance of events, it does not stand out by having great amplitudes. It is worth mentioning that the standard-deviation-threshold approach has been submitted to a sensitive test (successfully passed), in which the threshold was iteratively changed in order to validate the choice of the  $2\sigma$  range. The DOE and amplitude pattern was maintained throughout the test.

A very clear result is the notable increase of both amplitude and rate of occurrence of the events after 1999. Fig. 5 shows the total number of DOE throughout the 17 years analyzed for the three frequency bands highlighted in the spectrum of Fig. 3.

The most evident aspect is the marked increase of the number of occurrence of DOE per year from the year 1999 in the higher frequency band series of  $16.5^{-1}$  cpm. The number jumped from 6 events per year in 1998 to 60 in 1999, increasing even more in the following years to stabilize around 100 events per years from 2002 onward. The average number of DOE quadruples from 1993–1999 to 2000–2009 in that frequency band. The issue will be discussed in the next sections.

#### 4. Normal modes

Although the dominant frequencies of the harbor oscillations and their temporal variability have been characterized, their

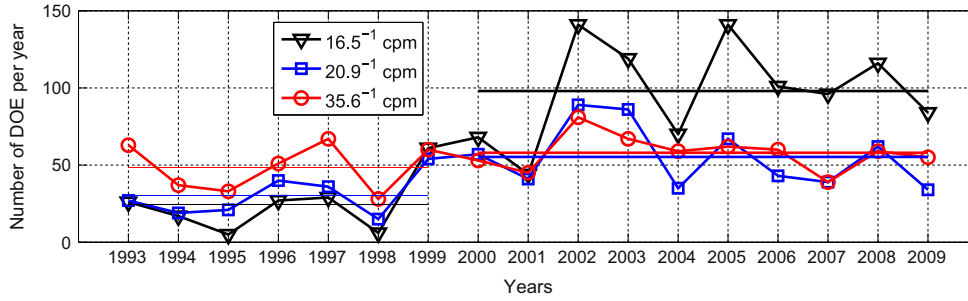


Fig. 5. Number of DOE per year for the three frequency bands discussed in the text. Thin lines are the averages of the periods 1993–1999 and 2000–2009, respectively.

nature has not been clarified. The spectrum in Fig. 3 exhibits three marked energy peaks at relatively isolated frequencies that are candidate to be related with resonant oscillations of the system. Resonant oscillations are standing waves supported by the harbor and, in the absence of friction and rotation, are given by the eigenvalue problem (Wilson, 1972; Delgado et al., 2011; Wang et al., 2011):

$$\frac{\partial}{\partial x} \left( H \frac{\partial \eta_j}{\partial x} \right) + \frac{\partial}{\partial y} \left( H \frac{\partial \eta_j}{\partial y} \right) + \left( \frac{\omega_j^2}{g} \right) \eta_j = 0, \quad j = 0, 1, 2, \dots \quad (1)$$

Here  $H$  is the bottom depth,  $g$  the gravity acceleration, and  $x, y$  denote the horizontal spatial coordinates. The eigenvalue is the wave angular frequency  $\omega_j$ , and the eigenfunction or spatial  $j$ th mode,  $\eta_j(x, y)$ , denotes the free surface vertical displacement. The prescribed boundary conditions for Eq. (1) are zero flux across the solid boundaries and the commonly assumed presence of a nodal line at the harbor mouth. In terms of  $\eta$  these conditions read

$$\frac{\partial \eta_j}{\partial n} = 0, \quad \eta_j = 0 \quad (2)$$

respectively, with  $n$  indicating the normal to the domain walls.

Following Rueda and Schladow (2002), Eqs. (1) and (2) have been solved by the Galerkin finite element method on the unstructured grid shown in Fig. 6a and b depicts the Helmholtz mode. It represents the simplest instance of resonant response (quarter-wave resonator) and describes an oscillation with a single nodal line at the harbor mouth and maximal amplitudes at its head (the antinode). Its period is the largest one among all the supported standing waves and in this case is  $T_0 = 16.5$  min, which agrees fairly well with the shorter period at which the observed spectrum presents a maximum. Any oscillation of greater period detected in the harbor, in particular those corresponding to the two energy peaks observed at periods of 20.9 min and 35.6 min, are expected to correspond to external signals rather than to resonant oscillations of the harbor.

The  $n=1$  mode (Fig. 6c) presents an additional nodal line at the narrower passage of the port, where the PdE1 tide gauge is located, and its period is  $T_1 = 6.2$  min. Any oscillation around this period should be hardly detected around this location, which is consistent with the fact that the PdE1 spectrum does not show significant energy at this frequency. The same reasoning will imply that the amplitudes around the location of PdE5 tide gauge cannot be null and, therefore, they should show up in the corresponding spectrum. Unfortunately, this result could not be confirmed by our data because  $T_1^{-1}$  is higher than the Nyquist frequency of the time series recorded by this tide gauge.

## 5. Resonance curve

Normal modes give natural frequencies and spatial patterns of the possible oscillations in the basin, but do not provide

information of the response to external forcing. Additionally, the previous calculation assumes the existence of a nodal line at the harbor mouth. While this is a reasonable approximation, the actual nodal line usually lies some distance outside the entrance, a fact that modifies to some extent the calculated resonant frequencies. Numerical models solving the primitive equations are useful in these regards (Dong et al., 2010).

A series of numerical experiments have been conducted in order to (1) study the sensitivity of the harbor response to the characteristics of incident long waves coming from the open sea, and (2) obtain an independent estimation of the spatial pattern and natural frequencies of the harbor normal modes. The model is based on a barotropic configuration of the MITgcm code (Marshall et al., 1997a,b), and its domain covers an area of  $6 \times 6$  km with the harbor in its northern part. For a given frequency,  $f_r$ , the model is laterally forced by a periodic velocity field such that it produces an overall sea surface oscillation of 1.5 cm amplitude (see details on model configuration and set up in Appendix A). This mimics the effect of remote atmospheric pressure perturbations of 1.5 hPa acting at frequency  $f_r$ .

First we have considered a forcing frequency  $f_r = 30^{-1} \text{ min}^{-1}$ . Fig. 7a shows the spectrum of the SSH at the head of the harbor and reveals the expected energy content at the forcing frequency,  $f_r$ , and also local maxima at  $f_0 = 16.55^{-1} \text{ min}^{-1}$  and  $f_1 = 7.05^{-1} \text{ min}^{-1}$ , this latter being less pronounced. The same response is found when the model is forced by other frequencies, as illustrated in Fig. 7b, which corresponds to a run with  $f_r = 10^{-1} \text{ min}^{-1}$ . Again, there is an energy maximum at the forcing frequency and also at  $f_0$  and  $f_1$ , with the latter now being more visible than in the previous case.

This strongly suggests resonance at  $f_0$  and  $f_1$  frequencies, and the agreement of these values with the calculated frequencies in Section 4 makes it clear that  $f_0$  and  $f_1$  correspond to the  $n=0$  and  $n=1$  resonant modes, respectively. The spatial structure of SSH amplitudes associated to these frequencies confirms this fact (see Fig. A1).

The amplification factor obtained for all the experiments is shown in Fig. 8 (asterisk marks), as a function of the forcing frequency. The maximum is reached at the Helmholtz frequency  $f_0 = 16.55^{-1} \text{ min}^{-1}$  with a factor of  $\sim 18$ , and decays relatively fast as one moves away from  $f_0$ . This resembles the behavior of a driven harmonic oscillator with small dissipation. In fact, our results agree with the theoretical amplification factor curve (see Rabinovich, 2009).

$$Af(f) = \left\{ \left[ 1 - \left( \frac{f_r}{f_0} \right)^2 \right]^2 + Q_f^{-2} \left( \frac{f_r}{f_0} \right)^2 \right\}^{-1/2} \quad (3)$$

which is plotted as a solid line in Fig. 8. In this expression  $Q_f$  is the so-called quality factor ( $Q$ -factor) and has been set to  $Q_f = 18$  in this case. The only worth noting discrepancy is the slight overestimation of  $A_f$  in the numerical experiments for  $f_r = 10^{-1}$  and  $f_r = 15^{-1} \text{ min}^{-1}$  with respect to the theoretical curve, which would

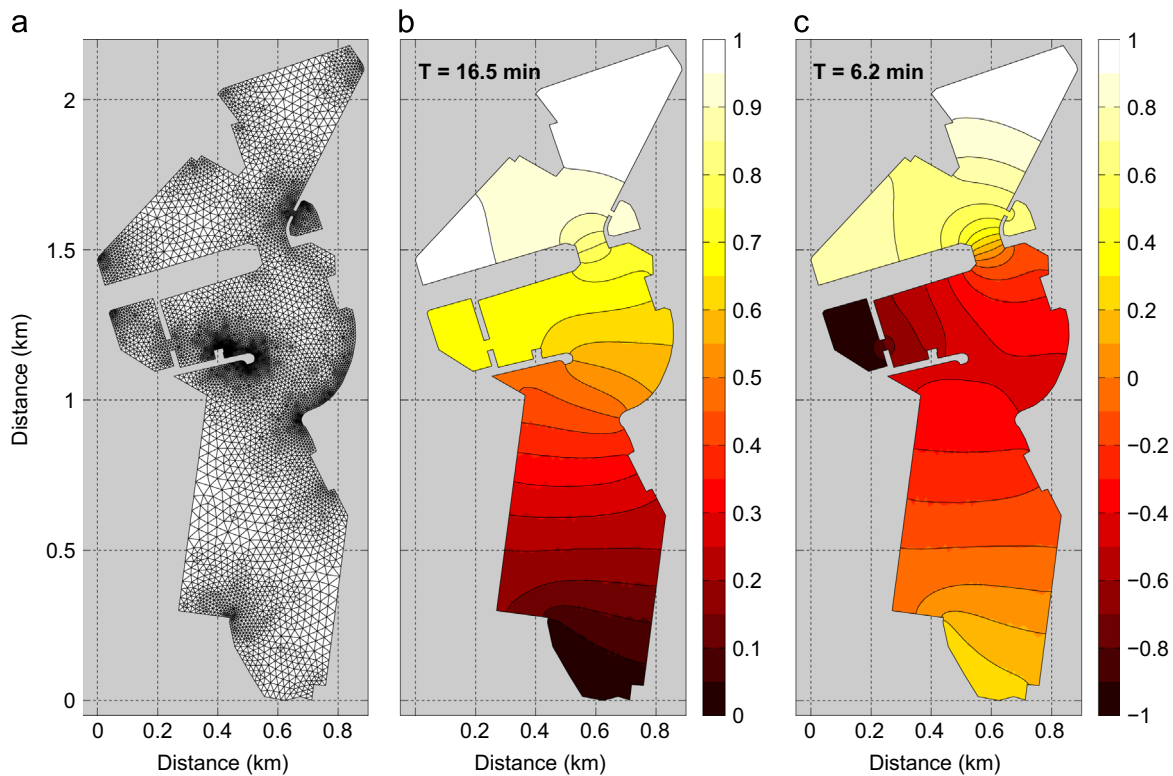


**Fig. 6.** Panel (a) finite element discretization grid used to solve the eigenvalue problem. Panel (b) and (c) amplitudes of the first and the second modes, respectively. Amplitude is expressed in normalized units.

be attributable to the proximity of these frequencies to the second resonant frequency  $f_1$ .

Comparatively to other similar settings, the Málaga harbor has a high  $Q$ -factor. For instance, the Ciutadella Inlet, in the Balearic Islands, where strong “rissaga” events occur, has an estimated  $Q$ -factor of  $\sim 10$  for the fundamental mode (Rabinovich et al., 1999; Monserrat et al., 1991), while the Malokurilsk Bay in the Shikotan Island (Japan), exhibits a  $Q$ -factor of  $\sim 13$  (Djumagaliev et al., 1994). The comparison has to be taken with caution, however, since in these cases the estimations were based on spectral methods applicable to monochromatic series rather than idealized numerical experiments (Rabinovich, 2009). Moreover, at least in the case of the Shikotan Islands, the observations were located at the entrance of the bay while our estimation is based on the averaged amplitude of the whole port domain.

## 6. Atmospheric forcing

The meteorological conditions for the occurrence of the short period oscillations characterized so far may differ from one event to the other and, moreover, are locally dependent. Fig. 9 shows the monthly distribution of the pressure anomaly during the events. Here the atmospheric pressure measured at the GOFIMA station has been low-pass filtered, its mean removed and the averaged anomalies of the 6 h before the event have been calculated.

The general tendency for the events is to coincide with low pressures (see the median value of the anomalies in Fig. 9, always below zero except in January) related with the transit of atmospheric systems (Monserrat and Thorpe, 1992; Monserrat et al., 2006). Atmospheric pressure anomaly and sea level variance are negatively correlated, the maximum correlation being  $-0.68$  with pressure leading the sea level oscillations by  $\sim 3.5$  h. That tendency is not a rule of thumb, however. Atmospheric pressure in spring/summer months is notably more stable and the events

occur almost always in low pressures, whereas the higher atmospheric pressure variability typical of the autumn and winter seasons induces an increase of the number of DOE under relatively high pressure.

Fig. 10 shows an example of harbor oscillations found in the band-pass filtered PdE1 series at  $16.5^{-1}$  cpm, where the sea level oscillations clearly exceeded 10 cm around the mean.

The oscillations occurred under low atmospheric pressure (anomalies are always negative), but the main forcing appears to be the high frequency disturbance of the barometric field triggered by the dramatic atmospheric pressure drop of 15 hPa in less than 1 h visible in Fig. 10, which took place shortly before the sea level oscillations.

Fig. 11 shows another fragment of the PdE1 band-pass filtered (at  $16.5^{-1}$  cpm) series representing the most energetic event detected. Sea level oscillations reach 20 cm (peak amplitude) around the mean, with a main wave train followed by a repetition of oscillations that weaken in the subsequent 8 h approximately. A peak in the variance of atmospheric pressure occurs approximately 3 h before, with weaker oscillations on its wake. The inset in the right upper corner of the figure shows the original series of sea level and atmospheric pressure and reveals a steep drop of 2.5 hPa in 45 min, which is followed by a series of high frequency oscillations of 0.4 hPa (peak) amplitude lasting for the whole lifetime of the sea level oscillations. It is worth noting that the short period sea level oscillations occurring during this -spring tide- tidal semi-cycle amply outweigh the tidal oscillations of the sea surface.

The correlation between pressure and sea level oscillations in the high frequency part of the spectrum has been assessed using a peak-to-peak, lag-based approach applied to the variance of both variables in the following manner: for each peak of the sea level variance a peak of pressure variance (defined using the same  $2\sigma$  threshold approach as in the case of the sea level variance) is sought for within a 12-h window previous to the event and, if the

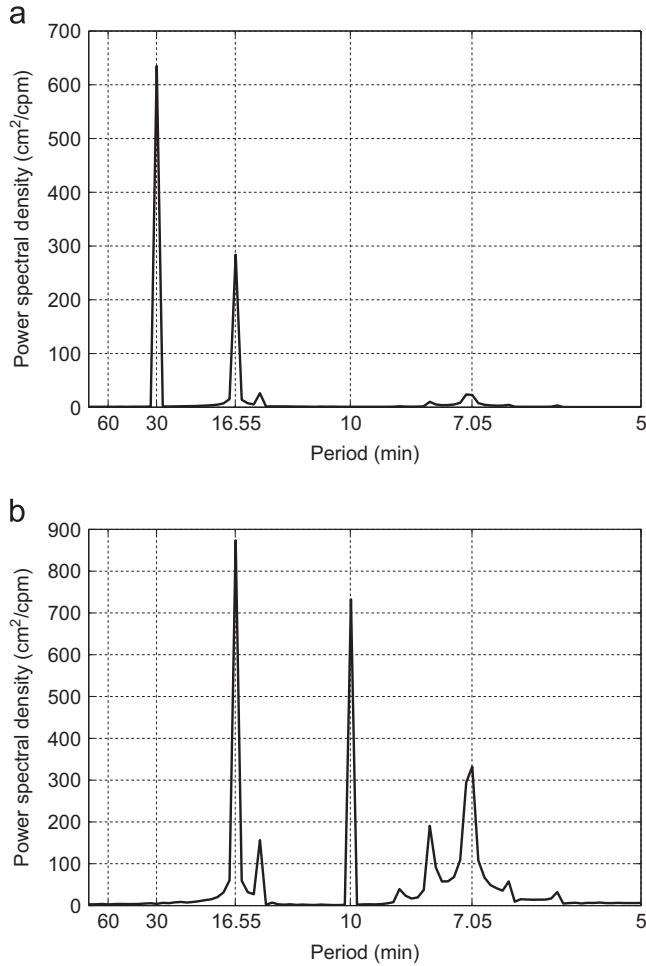


Fig. 7. Power spectra of the simulated sea level time series at one particular location of the head of the harbor. Panels (a) and (b) correspond to runs with forcing frequency  $f_r=30^{-1} \text{ min}^{-1}$  and  $f_r=10^{-1} \text{ min}^{-1}$ , respectively.

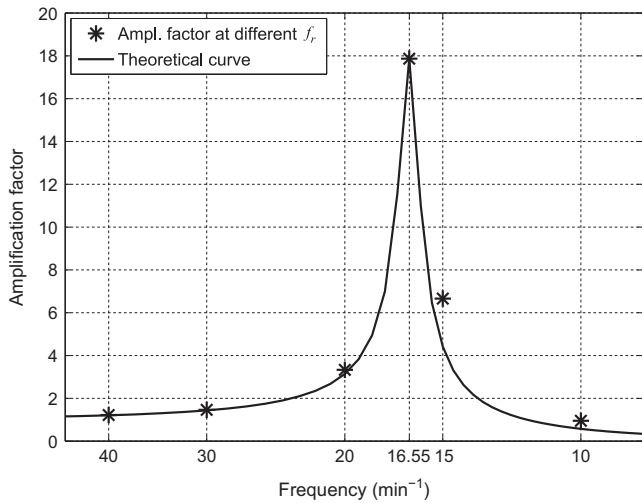


Fig. 8. Mean amplitude amplification factor for  $f_r=40^{-1}$ ,  $30^{-1}$ ,  $20^{-1}$ ,  $16.55^{-1}$ ,  $15^{-1}$ , and  $10^{-1} \text{ cpm}$  (asterisk marks). Solid line is the curved given by Eq. (3) for  $f_0=16.55^{-1} \text{ cpm}$ .

peak is found, the lag between both peaks is computed. The analysis shows that the peaks of pressure variance usually reflect the occurrence of a single pressure drop that is followed by bursts of high frequency atmospheric pressure fluctuations (it seldom happens that

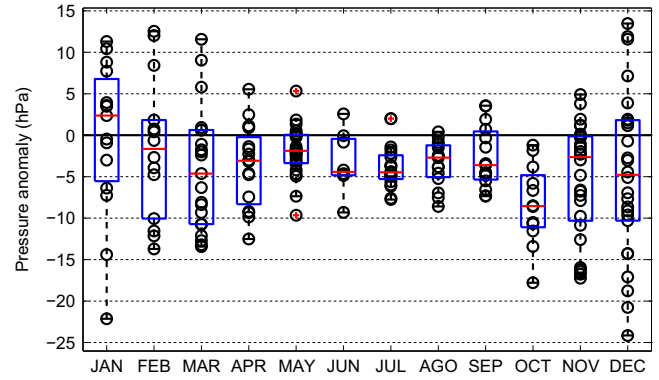


Fig. 9. Box-whiskers plot of pressure anomaly measured in GOFIMA station (see text for computation details) during the events. Median and inter quartile range are represented in red line and blue box, respectively. The whiskers extend to  $\pm 1.5$  times the inter quartile range, while the outliers (red crosses) are computed as the values exceeding these limits. Superimposed to the box-whiskers plot are the single values (black circles) of the pressure anomaly. (For interpretation of the references to color in this figure legend, the reader is referred to the web version of this article.)

these fluctuations are observed without a previous pressure drop). More than 70% of times, the identified peak of pressure variance was detected around 4 h before the event of sea level oscillations.

While pressure data recorded at GOFIMA station have proven to be useful to study the high frequency behavior of the barometric field, winds sampled in this station have poor angular resolution ( $22.5^\circ$ ) and are likely screened by the surrounding infrastructures. On the other hand, winds sampled by the AEMET stations have low temporal resolution to study such a highly variable field. These circumstances prevent us from doing a detailed analysis of the effect of the wind regimen on the short period sea level oscillations. Using the ASCAT dataset, which is free of local topographic effects, the observed sea level oscillations are observed under westerlies rather than under easterlies (65% versus 35%). Local topography usually changes the westerlies into north-westerlies, although in few cases of strong harbor oscillations (around 5% of the total events) they had veered into south-westerlies following the shoreline to the SW of the city (see for instance the event in Fig. 10).

### 7. Discussion and conclusion

The port of Málaga is routinely affected by short period oscillations whose amplitudes are of few cm as a rule, although they may eventually exceed 20 cm as illustrated in Fig. 11. Considering that the amplitude of M2 constituent is  $\sim 19 \text{ cm}$ , the short period oscillations are comparable or even may outweigh the tide during these extreme events when, therefore, they become relevant.

The spectra in Fig. 3 show three prevailing periods for these oscillations that stand out over a rather noisy background. The narrowness of the peaks is suggestive of harbor oscillations (Rabinovich, 2009), a reason that has motivated the analysis of the normal modes of the port. This has been carried out numerically using two different approaches. First, by solving the eigenvalue problem given by Eqs. (1) and (2) and, second, by analyzing the response inside the port provided by a barotropic model driven by external periodic forces (Appendix A).

Both independent approaches shed almost identical results for the spatial structure of the fundamental or Helmholtz mode (compare Fig. 6b and Fig. A1b) and the same fundamental frequency  $f_0=16.5^{-1} \text{ cpm}$ . It corresponds to the peak with the highest frequency of the three highlighted in Fig. 3, which indeed confirms that this is the frequency of the fundamental mode of the port. It is

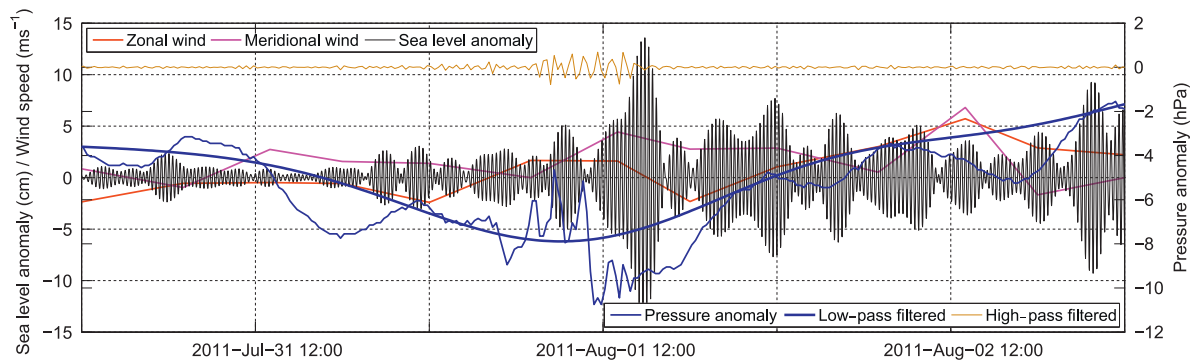


**Fig. 10.** A fragment of the PdE1 series band-pass filtered at  $16.5^{-1}$  cpm, with overlapped the two wind components measured in the PORT station and the pressure and its low-pass and high-pass filtered series, measured in GOFIMA station.

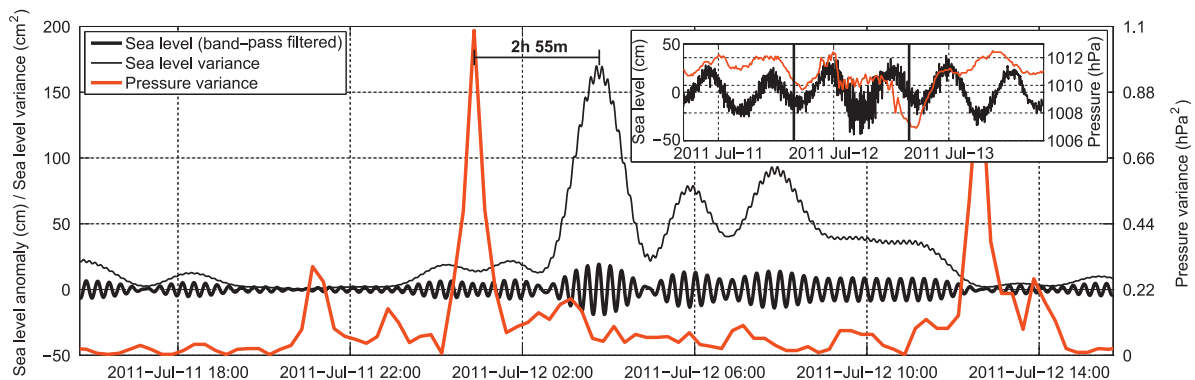


**Fig. 11.** Band-pass filtered (at  $16.5^{-1}$  cpm) sea level (thick black line), its corresponding variance (thin black line) and pressure variance (thick red line) by the GOFIMA series for the most energetic event found in the PdE1 series. Inset: unfiltered sea level (black) and pressure (red) for a slight larger period. Here the vertical thick bars indicate the temporal limits of the fragment displayed in the main graph. (For interpretation of the references to color in this figure legend, the reader is referred to the web version of this article.)

worth noting that the barotropic model predicts an amplification factor of 18 at this frequency (Fig. 8), which agrees well with the  $Q$ -factor  $Q = f_0/\Delta f$  deduced from the spectrum of Fig. 3 using the half-power bandwidth criterion (Emery and Thomson, 2001) and a  $\Delta f$  of  $0.8\text{--}0.9\text{ min}^{-1}$  from the figure. The coincidence provides robust arguments for the good performance of the model.

Similar conclusions are drawn for the second mode (Fig. 6c and Fig. A1c), although the frequencies differ slightly in this case ( $6.2^{-1}$  cpm against  $7.05^{-1}$  cpm). Despite its existence, the footprint of this mode is not visible in the spectra of Fig. 3 because the only tide gauge able to detect it (PdE1, whose sampling interval is 1) is placed at the narrowest part of the port (Fig. 1), where the mode has a nodal line. Neither approach indicate the existence of resonant modes with frequencies matching the  $20.9^{-1}$  and  $35.6^{-1}$  cpm peaks of Fig. 3, which suggests a different origin for them. This hypothesis is also supported by the fact that the structural reforms of the port completed in year 1999 increased the DOE per year dramatically for the  $16.5^{-1}$  cpm oscillations (which were virtually absent prior to this year, see Fig. 5) whereas hardly modified the number of DOE for the two other frequencies.

It has been shown repeatedly that the ultimate origin of harbor oscillations is the atmospheric forcing (Monserrat et al., 1991, 2006; Rabinovich, 2009). Both the AEMET and the GOFIMA records of atmospheric pressure have been used to characterize the prevailing meteorological conditions during the DOE, evaluating the low and high frequency behavior of the barometric field, respectively. These fields have been confronted with the time series corresponding to the port oscillations of 16.5 min period, which has been considered as representative of the Helmholtz mode of the harbor.

Although the occurrence of DOE coincides with low pressures, as shown in Figs. 10 or 11, it is not a rule of thumb. Around 25% of cases are observed when the atmospheric pressure is above its

mean, especially in winter months. The relevant point, however, is the notorious high frequency content in the atmospheric pressure records whenever short period oscillations are observed (see Fig. 10, for example), a feature that is common to almost all the events identified. A certain correlation with pressure disturbances, similar to the one observed for the fundamental frequency, is also found in the two other bands centered at  $20.9^{-1}$  and  $35.6^{-1}$  cpm, although the resulting amplitudes are quite weaker (roughly half and a quarter of the amplitude observed at the resonant frequency, respectively). The high frequency contribution, however, is not completely resolved in the 15-min-interval time series of GOFIMA, a fact that prevents the identification of the dominant frequency, if any. In any case, it is the advection of the disturbances by the atmospheric fronts that sweep the Iberian Peninsula from west to east that most likely triggers the harbor oscillations as they pass by.

With an amplitude of the atmospheric pressure disturbances typically  $O(1\text{ hPa})$ , the direct effect on the sea level would be oscillations of 1 cm amplitude under isostatic response, much less than the observed ones. However, the high  $Q$ -value of the port of Málaga ensures an amplified response if the atmospheric pressure disturbances contain frequencies closer to the Helmholtz mode. The process of amplification consists of two steps, as it has been reported repeatedly in the literature (Rabinovich, 2009; Monserrat et al., 2006). In a first step, atmospheric pressure disturbances transfer energy to the ocean at a much larger spatial scale than the harbor dimensions, for instance, by originating long ocean waves (Monserrat et al., 1991). Acting at the harbor's open mouth, these waves excite the harbor modes.

Two kinds of atmosphere-sea coupling can be invoked for an efficient atmosphere-to-sea energy transfer: the Greenspan and the Proudman resonances. The Greenspan resonance (Greenspan,

1956) occurs when the along-shore component of the velocity of the atmospheric disturbances matches the phase speed of some of the natural modes of the edge waves. Let us carry out some computations for a specific situation: during the event showed in Fig. 11, an atmospheric front was moving northeastward along the southern coast of the Iberian Peninsula. The displacement of a cloud mass in hourly EUMETSAT images (not shown) was used to make a guess of the speed of the front, which was estimated in  $\sim 16 \text{ m s}^{-1}$ , within the phase speed range of edge wave modes. Therefore, Greenspan resonance is a candidate mechanism for explaining this event (and others) of short period oscillations. Proudman resonance takes place when the phase speed of long oceanic waves equals the speed of the atmospheric pressure systems (Rabinovich, 2009). The phase speed of oceanic long waves,  $c = \sqrt{gH}$ , would match the progression speed of the front for  $H=25 \text{ m}$ , a representative depth for the inner continental shelf. Proudman resonance is thus another very feasible possibility for efficient energy transfer. Whichever the case, the excitation of the harbor oscillations requires the arrival of waves at the harbor's mouth containing energy in the frequency band centered around  $16.5^{-1} \text{ cpm}$  that must have been previously transferred from the atmosphere by any of the mentioned mechanisms. With no availability of any other kind of observations besides the ones previously discussed, we can only speculate with the fact that the two other observed bands centered at  $20.9^{-1}$  and  $35.6^{-1} \text{ cpm}$  have to be excited out of the port by any resonant mechanism similar to the ones described before. However, a set of further measurements in the nearby shelf would be required to corroborate this issue.

The effect of winds has also been addressed with inconclusive results. Although the events of short period oscillations are preferably observed under westerlies, it is also true that they occur with winds coming from other directions. The very large sampling interval of the available wind series (6 h) is clearly inadequate for addressing the issue properly.

## Acknowledgements

Model runs have been carried out in the supercomputer PICASSO by the Supercomputing and Bioinformatic Centre of the

University of Málaga. Partial financial support was provided by the Regional Andalusian Government (RNM137 and Proyecto de Excelencia RNM-1540). CN acknowledges the financial support within the action BES-1011-043421. JCSG acknowledges a postdoctoral fellowship (JCI-2012-13451) from the Spanish Ministry of Economy and Competitiveness. The authors are very grateful to the Spanish State Port Authority "Puertos del Estado" who kindly provided the sea level time series widely used in the work and especially to Pilar Gil Blázquez and Enrique Álvarez Fanjul for their kind collaboration. This is the publication no. 61 from CEIMAR Publication Series.

## Appendix: A. Resonant oscillations from a barotropic model

The procedure to derive the structure and natural frequencies of resonant oscillations in the harbor from a barotropic model simulation is described. The source code of the Massachusetts Institute of Technology General Circulation Model (MITgcm) is used to conduct our experiments. We are interested in long surface gravity waves, thus a free-surface, barotropic, and hydrostatic configuration of the model is applied. Additionally, the waves in question are linear (small-amplitude) and basically unaffected by the Earth's rotation (of much larger frequency than the inertial frequency), and therefore both the advective and the Coriolis terms are removed from the momentum equation. The model is initialized with sea water of constant density, and time-stepping for the tracer equations is also disabled in order to prevent unnecessary calculations. With this configuration the equations solved are the so-called shallow-water or barotropic long-wave equations.

The model domain has an area of  $6 \times 6 \text{ km}^2$  and has been discretized with a regular grid of  $x=y=10 \text{ m}$  resolution. In the vertical there is only one vertical level of variable thickness that fits the local bottom depth (partial-step representation of the bottom topography). At the solid boundaries no-slip boundary conditions are set. Additionally, explicit horizontal viscosity is included,  $\nu_H=1 \times 10^{-1} \text{ m}^2 \text{ s}^{-1}$ , and a quadratic bottom drag  $\tau=C_d\rho u^2$  has been imposed at the bottom boundary, with a drag coefficient  $C_d=2 \times 10^{-3}$ . This enables some energy dissipation in

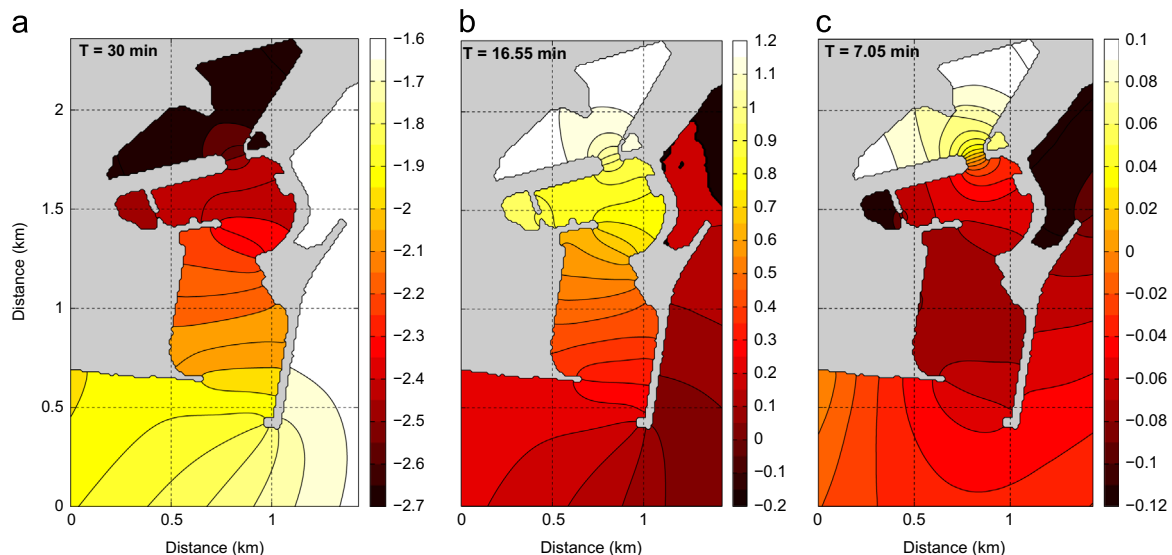


**Fig. A1.** Panels (a)  $A_r$ , (b)  $A_0$  and (c)  $A_1$  for the run with forcing frequency  $f_r=30^{-1} \text{ cpm}$ . Sea level amplitude is in cm. The amplitude sign is assigned depending upon the value of the corresponding phase, positive and negative for  $\phi_k=0$  and  $\phi_k=\pi$  ( $k=r, 0, 1$ ), respectively.

our model. The time step is set to  $\Delta t=0.1$  s, which satisfies the CFL stability condition for surface gravity waves.

The model is forced by prescribing the velocity field:

$$u = 0, \quad v = U \sin(2\pi ft);$$

$$u = -U \sin(2\pi ft), \quad v = 0;$$

at the southern and eastern open lateral boundaries, respectively. This produces an overall sea level oscillation of frequency  $f$  and amplitude

$$SSH_A = \frac{A_{lb}U}{2\pi f A_s}$$

where  $A_{lb}$  denotes the total area of the lateral boundaries (south plus east), and  $A_s$  is the area of the sea surface. In the following, for a given frequency  $f=f_r$ ,  $U$  is set so that  $SSH_A=1.5$  cm. This mimics the effect of remote atmospheric pressure perturbations of 1.5 hPa amplitude oscillating at the given frequency.

The experiment lasts for 8 h and the model outputs are written every minute. Consider, for instance the run corresponding to  $f_r=30^{-1} \text{ min}^{-1}$ . From the model outputs the resonant frequencies ( $f_0$  and  $f_1$ ) can be identified from the maxima of a SSH spectra, much like in Fig. A1.

To explore the spatial structure of SSH amplitudes at the frequencies of interest, the sea surface is expressed as:

$$SSH(x, y, t) = \overline{SSH}(x, y) + \sum_{k=r,0,1} A_k(x, y) \cos[2\pi f_k t + \phi_k(x, y)] + res$$

Here the bar denotes time-average and  $res$  is a (small) residue. SSH amplitude and phase,  $A_k$  and  $\phi_k$ , are obtained from the Fourier transform of the series. Fig. A1 shows  $A_k$  ( $k=r, 0, 1$ ), whose sign in every grid point has been assigned depending upon the value of the associated phase  $\phi_k$ ; positive and negative for  $\phi_k=0$  and  $\phi_k=\pi$ , respectively. These are the only values that phases take in the harbor and its surroundings.

$A_0$  maintains sign within the harbor, which means that the SSH oscillate in-phase. Amplitudes amplify towards the head of the harbor, and presents a nodal line lying some hundred meters away from its entrance.  $A_1$  also presents a nodal line outside the harbor, and a second one at the narrowest harbor passage. We can therefore state that  $A_0$  and  $A_1$  are the  $n=0$  (Helmholtz), and  $n=1$  resonant modes of the harbor, respectively.

Additionally, the amplification factor of the frequency  $f_r$  can be calculated from  $A_r$ . SSH oscillations have 1.5 cm amplitude outside the harbor, and the mean value of  $A_r$  within it is  $\sim 2.2$  cm, which implies a mean amplification factor of 1.46. It is important to note that the amplification factors derived here must be definitely sensitive to model parameters involving friction (bottom drag, side drag, and eddy viscosity coefficients). To this end, further runs, with different values of the drag coefficient, have been carried and results are fully satisfying. However, some further

tests may be desirable in the future to completely assess the sensitivity of the model for the amplification response. See Fig. A1.

## References

- Bentamy, A., Croize-Fillon, D., 2012. Gridded surface wind fields from Metop/ASCAT measurements. *Int. J. Remote Sens.* 6 (33) (17209–1754).
- Candela, J., et al., 1999. The “Mad Sea” phenomenon in the Strait of Sicily. *J. Phys. Oceanogr.* 29, 2210–2231.
- Chen, Guan-Yu, et al., 2004. Resonance induced by edge waves in Hua-Lien Harbor. *J. Oceanogr.* 60, 1035–1043.
- Delgado, J., et al., 2011. Short period sea level oscillations at Strait of Gibraltar: observations versus model results. *Estuarine Coastal Shelf Sci.* 95, 307–313 (2–3).
- Djumagaliev, V.A., Rabinovich, A.B., Fine, I.V., 1994. Theoretical and experimental estimation of transfer peculiarities of the Malokurilsk Bay coast, the Island of Shikotan Atmosph. Oceanic Phys. 30, 680–686.
- Drago, A., 2008. Numerical modelling of coastal seiches in Malta. *Phys. Chem. Earth* 33, 260–275 (3–4).
- Emery, W.J., Thomson, R.E., 2001. *Time-series Analysis Methods Data Analysis Methods in Physical Oceanography*. Elsevier Science, Amsterdam.
- Garcies, M., Gomis, D., Monserrat, S., 1996. Pressure-forced seiches of large amplitude in inlets of the Balearic Islands. Part II: Observational study. *J. Phys. Oceanogr.* 101, 6453–6467.
- Gomis, D., Monserrat, S., Tintoré, J., 1993. Pressure-forced seiches of large amplitude in. *J. Geophys. Res.* 98, 14437–14445.
- Greenspan, H.P., 1956. The generation of edge waves by moving pressure disturbances. *J. Fluid Mech.* 1, 574–592.
- Guohai, Dong, Gang, Wang, Ma, Xiaozhou, Yuxiang, Ma, 2010. Harbor resonance induced by subaerial landslide-generated impact waves. *Ocean Eng.* 37, 927–934.
- Hibiya, T., Kajiura, K., 1982. Origin of ‘Abiki’ phenomenon (kind of seiches) in Nagasaki Bay. *J. Oceanogr. Soc. Jpn.* 38, 172–182.
- Marshall, J., et al., 1997a. A finite-volume, incompressible Navier Stokes model for studies of the ocean on parallel computers. *J. Geophys. Res.* 102 (C3), 5753–5766.
- Marshall, J., et al., 1997b. Hydrostatic, quasi-hydrostatic, and nonhydrostatic ocean modeling. *J. Geophys. Res.* 102 (C3), 5733–5752.
- Monserrat, S., Thorpe, A.J., 1992. Gravity-wave observations using an array of microbarographs in the Balearic Islands. *Q. J. R. Meteorolog. Soc.* 118, 259–282.
- Monserrat, S., Ibbetson, A., Thorpe, A.J., 1991. Atmospheric gravity waves and the ‘rissaga’ phenomenon. *Q. J. R. Meteorolog. Soc.* 117, 553–570.
- Monserrat, S., Vilibic, I., Rabinovich, A.B., 2006. Meteotsunamis: atmospherically induced destructive ocean waves in the tsunami frequency band. *Nat. Hazards Earth Syst. Sci.* 6, 1035–1051.
- Muñoz, M.V., 1998. Análisis de las direcciones de los vientos en Andalucía. *Nimbus* 1, 153–168.
- Oenheim, A.V., Schafer, R.W., 1999. *Discrete-time Signal Processing*. - [s.l.]. Prentice Hall p. 879.
- Pawlowicz, R., Beardsley, B., Lentz, S., 2002. Classical tidal harmonic analysis including error estimates in MATLAB using T\_TIDE. *Comput. Geosci.* 28, 929–937.
- Rabinovich, A.B., Monserrat, S., Fine, I.V., 1999. Numerical modeling of extreme seiche oscillations in the region of Balearic Islands. *Oceanology* 39, 16–24.
- Rabinovich, A.B., 2009. *Seiches and Harbor Oscillations Handbook of Coastal and Ocean Engineering/book auth Kim Y. C.* World Scientific Publ., Singapore.
- Rueda, F., Schladow, S., 2002. Quantitative comparison of models for barotropic response of homogeneous basins. *J. Hydraul. Eng.* 128, 201–213 (2).
- Sawaragi, T., Kubo, M., 1982. The motions of a moored ship in a harbor basin, In: *Proc. of 18th Int. Conf. on Coastal, ASCE*, pp. 2743–2762.
- Wang, Gang, et al., 2011. An analytic investigation of oscillations within a harbor of constant slope. *Ocean Eng.*, 479–486.
- Wilson, B.W., 1972. *Seiches Advances in Hydrosceince/book auth. Chow Ven Te.* Academic Press, New York.